Climate
of the Past

Atlantic circulation changes across a stadial–interstadial transition

Claire Waelbroeck[1], **Jerry Tjiputra**[2], **Chuncheng Guo**[2], **Kerim H. Nisancioglu**[3], **Eystein Jansen**[2,3],
Natalia Vázquez Riveiros[4], **Samuel Toucanne**[4], **Frédérique Eynaud**[5], **Linda Rossignol**[5], **Fabien Dewilde**[6],
Elodie Marchès[7], **Susana Lebreiro**[8], and **Silvia Nave**[9]

[1]LOCEAN/IPSL, Sorbonne Université-CNRS-IRD-MNHN, UMR7159, 75005 Paris, France
[2]NORCE Norwegian Research Centre, Bjerknes Centre for Climate Research, 5007 Bergen, Norway
[3]Department of Earth Science, University of Bergen, Bjerknes Centre for Climate Research, 5007 Bergen, Norway
[4]Geo-Ocean, University of Brest, CNRS, IFREMER, UMR6538, 29280 Plouzané, France
[5]UMR-CNRS 5805 EPOC – OASU, University of Bordeaux, 50023 Pessac, France
[6]IUEM, UMS3113, 29280 Plouzané, France
[7]Service Hydrographique et Océanographique de la Marine, 29228 Brest, France
[8]Instituto Geológico y Minero de España (IGME)-CSIC, 28003 Madrid, Spain
[9]LNEG, I. P., UGHGC, 2610-999 Amadora, Portugal

Correspondence: Claire Waelbroeck (claire.waelbroeck@locean.ipsl.fr)

Abstract. We combine consistently dated benthic carbon isotopic records distributed over the entire Atlantic Ocean with numerical simulations performed by a glacial configuration of the Norwegian Earth System Model with active ocean biogeochemistry in order to interpret the observed *Cibicides* δ^{13}C changes at the stadial–interstadial transition corresponding to the end of Heinrich Stadial 4 (HS4) in terms of ocean circulation and remineralization changes. We show that the marked increase in *Cibicides* δ^{13}C observed at the end of HS4 between ~ 2000 and 4200 m in the Atlantic can be explained by changes in nutrient concentrations as simulated by the model in response to the halting of freshwater input in the high-latitude glacial North Atlantic. Our model results show that this *Cibicides* δ^{13}C signal is associated with changes in the ratio of southern-sourced (SSW) versus northern-sourced (NSW) water masses at the core sites, whereby SSW is replaced by NSW as a consequence of the resumption of deep-water formation in the northern North Atlantic and Nordic Seas after the freshwater input is halted. Our results further suggest that the contribution of ocean circulation changes to this signal increases from $\sim 40\%$ at 2000 m to $\sim 80\%$ at 4000 m. Below ~ 4200 m, the model shows little ocean circulation change but an increase in rem- ineralization across the transition marking the end of HS4. The simulated lower remineralization during stadials compared to during interstadials is particularly pronounced in deep subantarctic sites, in agreement with the decrease in the export production of carbon to the deep Southern Ocean during stadials found in previous studies.

1 Introduction

During the last glacial period, surface temperatures above Greenland and in the North Atlantic region shifted between cold (stadial) and warm (interstadial) phases. Previous studies have shown that these rapid changes in surface climatic conditions were accompanied by rapid changes in ocean circulation characterized by reduced Atlantic meridional overturning circulation (AMOC) during stadials (Vidal et al., 1997; Gottschalk et al., 2015; Waelbroeck et al., 2018; Toucanne et al., 2021). However, the precise geometry and extent of Atlantic circulation changes are still under debate due to the scarcity of available observations and the large dating uncertainties of marine sediment records.

Among the proxy data that can be used to reconstruct past changes in ocean circulation, benthic foraminiferal oxygen (δ^{18}O, expressed as an anomaly relative to a standard in ‰ versus Vienna Pee Dee Belemnite, VPDB) and carbon (δ^{13}C, expressed in ‰ versus VPDB) isotopes offer the best spatial and temporal coverage. However, these proxies do not solely record ocean circulation changes and depend on several factors that complicate their interpretation. At present, the extraction of the ocean circulation signals out of benthic δ^{18}O and δ^{13}C records remains a relevant objective which has the potential to significantly improve our understanding of the ocean processes at play during the rapid climate changes of the last glacial and deglaciation periods.

Over the past 25 years, it has been shown that a decrease in benthic δ^{13}C took place in the Atlantic Ocean during Heinrich stadials, whose amplitude depends on the location and water depth of the cores. This decrease in benthic δ^{13}C has been classically interpreted as a reflection of a decrease in northern-sourced water (NSW) formation and a concomitant increase in the southern-sourced water (SSW) fraction (Willamowski and Zahn, 2000; Elliot et al., 2002; Skinner and Shackleton, 2006; Peck et al., 2006, 2007). However, more recent studies also suggested that this decrease in benthic δ^{13}C could be due to a decrease in NSW δ^{13}C preformed value (Waelbroeck et al., 2011; Crocker et al., 2016; Lund et al., 2015) or an increase in organic matter remineralization (Hoogakker et al., 2007; Lacerra et al., 2017; Voigt et al., 2017) or a combination of these factors and of an increase in the SSW fraction (Oppo et al., 2015).

Other ocean circulation proxies include sedimentary Pa/Th, sortable silt, neodymium isotopic composition, benthic foraminiferal Ba/Ca, and Cd/Ca (Lynch-Stieglitz and Marchitto, 2014). However, caveats about each of these proxies, combined with the scarcity of well-resolved records of the last glacial millennial changes, have not permitted the reconstruction of 3-D changes in ocean water masses distribution associated with the rapid climate changes of the last glacial.

In such a context, isotope-enabled models appear to be extremely useful tools for disentangling the different factors that influence the benthic δ^{13}C signal and for producing 3-D pictures of the ocean circulation changes. Such models have been mainly used to simulate pre-industrial (PI) (Schmittner et al., 2013; Menviel et al., 2015) or Last Glacial Maximum (LGM; Menviel et al., 2017, 2020; Muglia et al., 2018; Muglia and Schmittner, 2021; Morée et al., 2021) conditions. A few studies with isotope-enabled models have addressed ocean circulation changes induced by hosing experiments mimicking stadial–interstadial transitions under PI boundary conditions (Schmittner and Lund, 2015; Missiaen et al., 2020). To our knowledge, there has been only one study using a transient simulation with carbon isotopes initialized under glacial conditions (Gu et al., 2021). This study focused on the mid-depth (1500–2500 m) Atlantic δ^{13}C decrease observed across the transition from the LGM to Heinrich Sta-

dial 1 and concluded that this decrease is mainly explained by increased remineralization due to AMOC slowdown, while the water mass mixture change only plays a minor role (Gu et al., 2021).

Here, we combine consistently dated benthic carbon isotopic records distributed over the Atlantic Ocean with numerical simulations performed by a glacial configuration of the Norwegian Earth System Model (NorESM) with active ocean biogeochemistry, and we investigate the changes observed in the *Cibicides* δ^{13}C records across the stadial–interstadial transition corresponding to the end of Heinrich Stadial 4 (HS4). This climate transition, dated at 38.17 ± 0.73 ka, is characterized by a rapid increase in Greenland and North Atlantic surface temperatures, leading from HS4 to Greenland Interstadial 8 (GI8) conditions (Rasmussen et al., 2014; Waelbroeck et al., 2019). This transition is particularly interesting because it is the largest and best-expressed transition in the *Cibicides* δ^{13}C records prior to the last deglaciation. It thus offers a case study of a rapid and large climatic transition away from large changes in insolation and greenhouse gases. Therefore, one can assume that the recorded climate and ocean circulation changes across the HS4-to-GI8 transition are not driven by changes in the radiative forcing. This reduces the dynamical complexity and makes the use of a hosing experiment under constant radiative forcing adequate to interpret the observed changes in the proxy records.

Our study provides a 3-D picture of the ocean circulation changes across this stadial–interstadial transition anchored in *Cibicides* δ^{13}C observations distributed between 2000 and 5000 m depth. We decompose the non-sea-air component of the δ^{13}C change across the HS4-to-GI8 transition into a fraction due to remineralization changes and the remaining fraction due to changes in water mass origin and geometry. Our results show that the non-sea-air δ^{13}C change across the HS4-to-GI8 transition due to remineralization changes decreases with increasing water depth and that, below $\sim$ 3000 m, the replacement of SSW by NSW plays a dominant role.

2 Material and methods

2.1 Observations

2.1.1 Benthic carbon isotopes

The δ^{13}C isotopic ratio of the epifaunal benthic foraminifer genus *Cibicides* (noted as *Cib.* hereafter) has been shown to record the δ^{13}C of bottom-water dissolved inorganic carbon (DIC), δ^{13}C-DIC, with minor isotopic fractionation (Duplessy et al., 1984; Zahn et al., 1986; Schmittner et al., 2017). The initial DIC isotopic composition of a given water mass is governed by surface productivity in its formation region (i.e., the preferential consumption of ^{12}C by primary productivity, thereby increasing dissolved δ^{13}C), as well as by temperature-dependent air–sea exchanges (Lynch-Stieglitz et

al., 1995). The δ^{13}C-DIC subsequently decreases as deep water ages due to the progressive remineralization at depth of relatively ^{13}C-depleted biogenic material. As a result, δ^{13}C-DIC largely follows water mass structure and circulation in the modern ocean, and *Cib.* δ^{13}C has been used to trace water masses and as a proxy of bottom-water ventilation (Duplessy et al., 1988, and numerous subsequent studies).

In short, δ^{13}C-DIC is driven by the biological activity (i.e., photosynthesis and remineralization) on the one hand and by thermodynamic fractionation during air–sea exchanges on the other hand.

A recent reconstruction of the pre-industrial δ^{13}C-DIC distribution and of its partitioning into biological and thermodynamic components shows that the former term prevails below 2000 m, with the air–sea δ^{13}C component ranging from -0.4 ‰ VPDB in the North Atlantic to $+0.2$ ‰ in the Southern Ocean, which is in contrast to the biological δ^{13}C component that ranges from $+1.4$ ‰ PDB in the North Atlantic to $+0.4$ ‰ in the Southern Ocean (Eide et al., 2017).

2.1.2 *Cibicides* δ^{13}C time series

A set of 110 consistently dated foraminifer isotopic records was built during the ACCLIMATE project making use of the PARIS database structure (Lougheed et al., 2022). Among these 110 cores, 92 could be directly dated according to the approach described in Waelbroeck et al. (2019), but the age models of the remaining cores had to be established by alignment to some of the directly dated cores, thereby introducing additional dating uncertainties.

For the purposes of the present study, the dated *Cib.* δ^{13}C records were screened in order to retain only sufficiently well-resolved (average time step of 100 to 500 years in most cases and smaller than 750 years in two cases) and well-dated *Cib.* δ^{13}C records in the vicinity of the HS4-to-GI8 stadial–interstadial transition. Therefore, only cores with relatively precise chronological information at the end of HS4 were retained – that is, cores that presented a radiocarbon date or an alignment tie point at the end of HS4, whose calendar age has a 1σ dating uncertainty lower than 1000 years.

Applying this screening criteria to the 110 ACCLIMATE cores, we are left with only 18 *Cib.* δ^{13}C records (Table S1 in the Supplement). Among the selected 18 *Cib.* δ^{13}C records, 6 are new records which were generated during the ACCLIMATE project (Sect. S1 in the Supplement). In terms of dating, six cores could not be directly dated but were aligned to one of the previously published cores (Waelbroeck et al., 2019) taken as a reference. Also, the age models of 4 of the remaining 12 cores have been improved with respect to the age model published in 2019. The reader is referred to Sect. S2 for detailed information on the dating.

2.2 Numerical experiment

In this study, we took advantage of a fast version of NorESM, NorESM1-F (Guo et al., 2019a), which features a horizontal resolution of about $2°$ in the atmosphere and nominal $1°$ in the ocean and sea ice. The computational efficiency of the model allows the experiments to be integrated for multiple millennia within a reasonable wall clock time. The NorESM1-F model with active ocean biogeochemistry has been used in several studies to investigate changes in the ocean circulation and carbon cycle (Kessler et al., 2018; Galaasen et al., 2020).

The NorESM glacial simulations reported in this study are based on previous work by Guo et al. (2019b) and Jansen et al. (2020). To briefly summarize, we performed an equilibrium simulation of the last glacial period forced by the boundary conditions of 38 ka, which corresponds to the beginning of GI8. The boundary conditions are different from the present day in terms of orbital forcing, greenhouse gases (CO_2, CH_4, and N_2O), land–sea mask, and the height and extent of the global ice sheets. Details of the configuration and simulation results of the physical climate are documented in Guo et al. (2019b).

The physical climate reached a stable interstadial state after 2500 model years, as shown by Guo et al. (2019b). From this point, we activated the full coupling of the physical components of NorESM1-F with its ocean biogeochemical (BGC) component (HAMOCC; Tjiputra et al., 2020) that is initialized from present-day climatology (including PO_4, NO_3, oxygen, dissolved inorganic carbon, and alkalinity; Key et al., 2004; Garcia et al., 2010a, b). Due to the long equilibration timescales of BGC tracers and the difference between glacial and present-day climate states, we continued the integration for another 2510 years (e.g., until model year 5010) to ensure that the BGC tracers are in a satisfactory quasi-equilibrium state. This ~ 2500-year length of the simulation with the BGC component activated is a compromise between demanding computing time and the relatively long time period (e.g., multiple millennia) required for ocean physics and BGC fields to reach a quasi-equilibrium state. More specifically, we consider the quasi-equilibrium state of the BGC fields to be satisfactory when the residual BGC drift is substantially smaller than the signal induced by freshwater forcing (on the order of a few percent).

Next, we branched off from the simulation above and applied a freshwater-hosing method to force the interstadial climate state into a cold stadial state. The freshwater is evenly distributed between 50 and $70°$ N, with an injection of 0.33 Sv ($1\,\text{Sv} = 10^6\,\text{m}^3\,\text{s}^{-1}$) for 800 years (i.e., until model year 5810), during which time a full stadial-like state (with a weak and shallow AMOC and an extensive sea ice cover in the North Atlantic) is achieved in the early phase of the simulation with freshwater forcing. We subsequently stopped the freshwater input to study the cold-to-warm transition process of the climate system. The model simulation of

recovery (i.e., without freshwater forcing) lasted for another 400 years (i.e., until model year 6210).

The freshwater simulation and transition process of the physical climate system is partly documented by Jansen et al. (2020). Note that the freshwater input lasted for only 500 years in that study; however, the dynamics of the physical climate processes during the transition are quite similar with the two forcing time lengths. In this study, we extend the forcing length to 800 years in order to (1) better match the observed length of HS4 (Wolff et al., 2010; Waelbroeck et al., 2019) and (2) achieve a better-equilibrated deep Atlantic Ocean during the stadial state.

As shown by Jansen et al. (2020), NorESM1-F provides a robust representation of the HS4-to-GI8 transition process, both in terms of the magnitude ($\sim 10\,°C$) and rate (nearly $1\,°C$ per decade) of temperature change when comparing to Greenland ice core records (see Fig. 3 of Jansen et al., 2020). The transition process takes about 100 years to complete, after which the climate returns to an interstadial state close to the pre-hosing period. Further dynamical processes and sequences of events in the climate system that occurred during the transition, including favorable agreement with sea surface and subsurface temperature and sea ice records in the Nordic Seas and North Atlantic, will be presented in a more detailed study (Guo, 2023). The focus of the present study is on the change in ocean circulation as revealed by the observed and simulated distribution of nutrient and BGC tracers.

2.3 Simulated tracers

As explained above, δ^{13}C-DIC can be decomposed into biological and air–sea exchange components. Using the approach of Broecker and Maier-Reimer (1992), we can compute the biological component (termed δ^{13}C-BIO hereafter) of the δ^{13}C-DIC as a linear function of the simulated phosphate concentration, PO$_4$:

$$\delta^{13}\text{C-BIO} - \delta^{13}\text{C}_{\text{mean o}} = \frac{\alpha\_\text{photo}}{\text{DIC}_{\text{mean o}}} \cdot \frac{\text{C}}{\text{P}}$$
$$\cdot (\text{PO}_4 - \text{PO}_{4\,\text{mean o}}), \qquad (1)$$

where $\alpha\_$photo is the carbon isotopic fractionation during photosynthesis; C/P is the ocean mean carbon-to-phosphorus ratio; and δ^{13}C$_{\text{mean o}}$, DIC$_{\text{mean o}}$, and PO$_{4\,\text{mean o}}$ are the mean ocean δ^{13}C, DIC, and PO$_4$, respectively.

We take $\alpha\_$photo $= -19\,‰$ (Broecker and Maier-Reimer, 1992) and C/P $= 122$ (Takahashi et al., 1985), both of which can be assumed to be constant in time. We take δ^{13}C$_{\text{mean o}} = 0.14\,‰$ VPDB, as estimated for the glacial ocean (Gebbie et al., 2015). We apply DIC$_{\text{mean o}} = 2188.4\,\mu\text{mol}\,\text{kg}^{-1}$ and PO$_{4\,\text{mean o}} = 1.7483\,\mu\text{mol}\,\text{kg}^{-1}$, taken as the long-term mean values of the MIS3 model simulation.

The NorESM1-F model is not isotope-enabled, so in this study, we focus on water depths below 2000 m and use δ^{13}C-BIO as an approximation of δ^{13}C-DIC. At the pre-industrial,

this approximation yields slightly overestimated δ^{13}C-DIC values in the North Atlantic (by $0.0\,‰$–$0.4\,‰$) and slightly underestimated δ^{13}C-DIC values in the Southern Ocean (by $0.0\,‰$–$0.2\,‰$; Eide et al., 2017). So, not surprisingly, we find offsets between the simulated δ^{13}C-BIO and observed *Cib.* δ^{13}C values (Fig. S1 in the Supplement). Were the model perfect, these offsets would correspond to the air–sea component of δ^{13}C-DIC during the simulated interstadial and subsequent hosing experiment.

In this study, we circumvent the existence of these offsets by comparing the simulated change in δ^{13}C-BIO to the observed change in *Cib.* δ^{13}C across the HS4-to-GI8 transition rather than the computed δ^{13}C-BIO and the observed *Cib.* δ^{13}C values during the HS4 and GI8 time intervals, respectively. Furthermore, we minimize the errors resulting from the non-inclusion of the air–sea component of δ^{13}C-DIC by retaining only core sites located below 2000 m.

In addition to nutrients and carbon tracers, the NorESM1-F model provides preformed tracers, such as the preformed phosphate (PO$_4^{\text{pre}}$), DIC, or dissolved oxygen (Guo et al., 2019a; Tjiputra et al., 2020). The preformed concentration of a tracer is defined as the concentration of this tracer in a parcel of water the last time this parcel was at the ocean surface. A tracer can thus be separated into its preformed concentration and its regenerated concentration, i.e., the concentration resulting from biological remineralization in the interior of the ocean (Duteil et al., 2012; Bernardello et al., 2014). For instance, preformed phosphate reflects the amount of phosphate returning to the ocean interior by physical processes (Duteil et al., 2012).

At any location below the ocean mixed layer, the total PO$_4$ concentration can thus be expressed as the sum of two terms as follows:

$$\text{PO}_4 = \text{PO}_4^{\text{pre}} + \text{PO}_4^{\text{rem}}, \qquad (2)$$

where PO$_4^{\text{rem}}$ is the amount of PO$_4$ locally produced by organic matter remineralization.

In the NorESM1-F model, preformed tracers are set to their respective total values in the ocean mixed layer (i.e., the upper two levels of the ocean model) at each time step. Below, the preformed tracers are advected as passive (i.e., conservative) tracers by the ocean circulation (Tjiputra et al., 2020). They can thus be used to track changes in ocean circulation and water mass geometry below the surface ocean.

In this study, we use the preformed PO$_4$ computed by NorESM1-F to deconvolve the GI8–HS4 δ^{13}C-BIO change, $\Delta\delta^{13}$C-BIO, into a fraction resulting from remineralization changes and the remainder, i.e., changes in primary production (PP) in the surface ocean and changes in ocean circulation. Importantly, in what follows, we use the term ocean circulation changes to refer to all the ocean circulation changes that are reflected by water mass tracers – that is, the changes in water mass origin and geometry but not the changes in water mass flow rate. The latter are reflected in the computed ideal age of the water mass, defined as the time since the

water mass last made contact with the surface (Guo et al., 2019b).

Combining Eqs. (1) and (2) and subtracting HS4 values from GI8 values, we obtain

$$\Delta \delta^{13}\text{C-BIO} = \frac{\alpha_{\text{photo}}}{\text{DIC}_{\text{mean o}}} \cdot \frac{C}{P} \cdot \left(\Delta PO_4^{\text{pre}} + \Delta PO_4^{\text{rem}}\right)$$
$$= \left(\Delta \delta^{13}\text{C-BIO}\right)_{\text{circ+PP}} + \left(\Delta \delta^{13}\text{C-BIO}\right)_{\text{rem}}, \quad (3)$$

where $(\Delta \delta^{13}\text{C-BIO})_{\text{circ+PP}}$ is the portion of $\Delta \delta^{13}\text{C-BIO}$ resulting from ocean circulation and surface PP changes, and $(\Delta \delta^{13}\text{C-BIO})_{\text{rem}}$ is the portion of $\Delta \delta^{13}\text{C-BIO}$ resulting from remineralization changes in the ocean interior.

3 Results

In order to compare the simulated GI8–HS4 change in δ^{13}C-BIO with the observed change in $Cib.$ δ^{13}C, we compute the mean observed and simulated values just before and just after the transition. Model outputs are averaged over a 100-year pre-transition stadial period and a 100-year post-transition interstadial period, respectively defined as model years 5700–5800 of the simulation with freshwater forcing and model years 5950–6050 of the simulation in which the freshwater input has been halted. These two time intervals correspond to relatively stable conditions, as attested by the low standard deviations of the simulated values within each interval (Table S2).

Due to the much-lower temporal resolution of the $Cib.$ δ^{13}C proxy records compared to the yearly model output, we average the $Cib.$ δ^{13}C records over 500-year periods to increase the number of records included in the study. Hence, HS4 and GI8 $Cib.$ δ^{13}C are averaged over the 38.5–39.0 and 37.5–38.0 ka intervals, respectively (Table 1). We estimate the uncertainty associated with these HS4 and GI8 $Cib.$ δ^{13}C values by combining the uncertainty resulting from the dispersion of the $Cib.$ δ^{13}C measurements within the 500-year intervals and the dating uncertainty (see Sect. S3 for more details).

Among the 18 selected sites (Figs. 1 and S1, Table 1), we obtain a strict agreement between the change in simulated δ^{13}C-BIO and the observed $Cib.$ δ^{13}C in 10 out of 18 sites within $\pm 1\sigma$ (blue symbols in Fig. 1). In five out of the remaining eight sites, the simulated trend in δ^{13}C-BIO is consistent with that in $Cib.$ δ^{13}C, but the model underestimates the GI8–HS4 $Cib.$ δ^{13}C change (green symbols in Fig. 1). Finally, simulated δ^{13}C-BIO and observed $Cib.$ δ^{13}C changes disagree in three sites (red symbols in Fig. 1). A regression analysis of $\Delta \delta^{13}$C-BIO versus $\Delta Cib.$ δ^{13}C values for (i) all sites, (ii) only sites depicted in blue and green, and (iii) only sites depicted in blue shows that the linear regressions are all highly significant, with probabilities of no linear correlation lower than 0.007 in all three cases and correlation coefficients (Pearson's) ranging from 0.63 to 0.82 from case (i) to (iii) (Fig. S2).
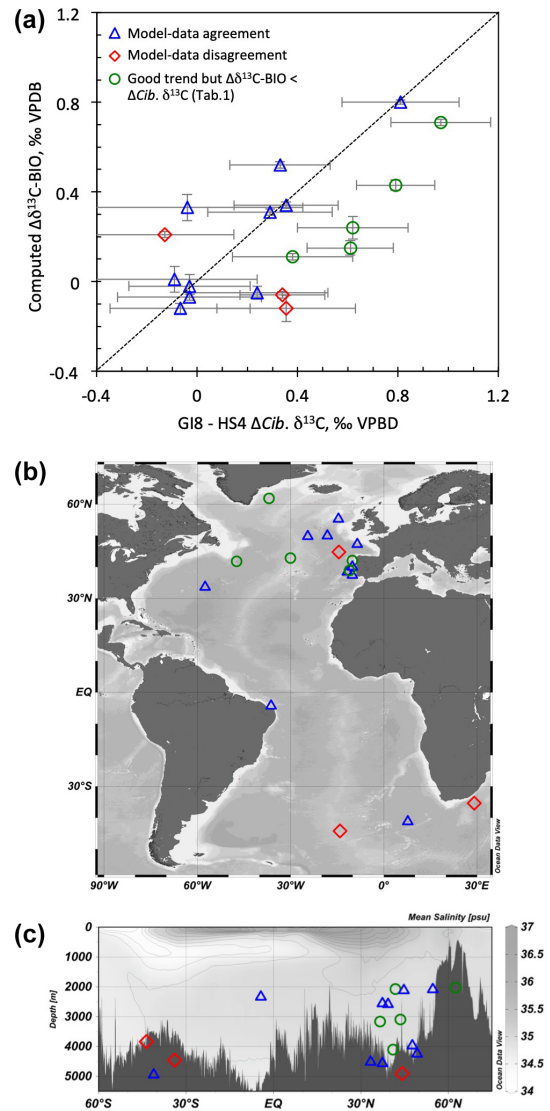

Figure 1. (a) Change in δ^{13}C-BIO simulated by NorESM1-F versus observed change in $Cib.$ δ^{13}C across the HS4-to-GI8 transition. Plotted error bars are $\pm 1\sigma$. **(b, c)** Position of the different core sites.

Among the three sites exhibiting model–data disagreement (red symbols), two are from the southeast Atlantic (Fig. 1). It is noteworthy that the southeast Atlantic Ocean is a problematic region for epibenthic isotopic time series for the following two reasons: (i) dating is difficult due to variable surface reservoir ages and the lack of sharp temperature changes in the Antarctic ice core records that can serve as alignment targets for sea surface temperature records; and (ii) the glacial δ^{13}C value of the epibenthic genus $Cibicides$ has been shown to be much lower for the species $Cibicides$ $kullenbergi$ than for the species $Cibicides$ $wuellerstorfi$ in certain instances (Gottschalk et al., 2016b), pointing to different habitat preferences for these two species and the presence of local phytodetritus layers on the sediment–water interface, possibly

Table 1. Partitioning of computed δ^{13}C-BIO changes across the HS4–GI8 transition, $\Delta\delta^{13}$C-BIO, into $(\Delta\delta^{13}$C-BIO$)_{\text{circ}+\text{PP}}$ and $(\Delta\delta^{13}$C-BIO$)_{\text{rem}}$ components (Eq. 3).

Core*	Depth, m	Latitude, decimals	Longitude, decimals	$\Delta Cib.$ δ^{13}C, ‰	± 1σ, ‰	$\Delta\delta^{13}$C-BIO, ‰	± 1σ, ‰	$(\Delta\delta^{13}$C-BIO$)_{\text{circ}+\text{PP}}$, ‰	± 1σ, ‰	% $\Delta\delta^{13}$C-BIO from circulation + PP changes	$(\Delta\delta^{13}$C-BIO$)_{\text{rem}}$, ‰	± 1σ, ‰
SU90-24	2085	62.07	-37.03	**0.79**	0.16	**0.43**	0.02	**0.19**	0.01	44	**0.24**	0.03
MD99-2331	2120	42.15	-9.68	**0.38**	0.24	**0.11**	0.01	**0.03**	0.01	27	**0.08**	0.02
NA87-22	2161	55.50	-14.70	**0.33**	0.20	**0.52**	0.01	**0.23**	0.01	44	**0.29**	0.02
MD13-3438	2124	47.45	-8.45	**0.35**	0.21	**0.34**	0.01	**0.16**	0.01	47	**0.18**	0.02
GeoB3910	2344	-4.24	-36.35	**0.81**	0.23	**0.80**	0.02	**0.43**	0.01	54	**0.37**	0.03
MD01-2444	2460	37.55	-10.13	**0.29**	0.25	**0.31**	0.02	**0.19**	0.00	61	**0.12**	0.02
MD95-2040	2465	40.58	-9.86	-0.04	0.46	**0.33**	0.01	**0.20**	0.00	61	**0.13**	0.01
SU90-08	3080	43.05	-30.04	**0.97**	0.20	**0.71**	0.01	**0.37**	0.01	52	**0.34**	0.02
MD95-2042	3146	37.80	-10.17	**0.61**	0.17	**0.15**	0.03	**0.11**	0.02	73	**0.04**	0.04
MD07-3076Q	3770	-44.15	-14.22	-0.13	0.28	**0.21**	0.01	**0.19**	0.02	90	0.02	0.02
U1308	3883	49.88	-24.23	-0.09	0.33	0.01	0.06	**0.03**	0.02	--	-0.02	0.06
CH69-K09	4100	41.76	-47.35	**0.62**	0.22	**0.24**	0.05	**0.17**	0.03	71	**0.07**	0.06
SU90-44	4255	50.10	-17.91	0.24	0.28	**-0.05**	0.03	-0.01	0.02	--	-0.04	0.04
MD16-3511Q	4435	-35.36	29.24	**0.34**	0.17	**-0.06**	0.01	**0.08**	0.01	-133	**-0.14**	0.02
KNR191-CDH19	4541	33.69	-57.58	-0.03	0.24	-0.02	0.02	**0.02**	0.01	-100	**-0.04**	0.02
MD03-2698	4602	38.24	-10.39	-0.03	0.29	**-0.07**	0.04	-0.01	**0.01**	14	-0.06	0.04
CAR13-05	4870	45.00	-14.33	**0.36**	0.28	**-0.12**	0.06	-0.03	0.02	25	-0.09	0.06
TNO57-21	4981	-41.10	7.80	-0.07	0.28	**-0.12**	0.04	**0.06**	0.01	-50	**-0.18**	0.05

* Cores are ordered by increasing water depths and are separated into two groups: above and below 4200 m (see text). Green indicates a good trend, but the computed GI8-HS4 δ^{13}C-BIO is smaller than the observed amplitude; red indicates model–data disagreement; bolding indicates significant changes.

with very low δ^{13}C-DIC values (Mackensen et al., 1993). The third site where observed and computed δ^{13}C amplitudes disagree, CAR13-05, is located in the northeast Atlantic (Table 1). Although it passed the screening test for dating quality, its sedimentation rate is relatively low over the studied time interval (6 to 10 cm kyr^{-1}; Fig. S3). The closest core in terms of latitude, longitude, and water depth, MD03-2698 (Table 1), has a sedimentation rate of about 50 cm kyr^{-1} (Fig. S3) and shows an excellent data–model agreement. Since marine sediment core age model precision and reliability are much improved for higher sedimentation rates, we may consider it to be that the GI8–HS4 *Cib.* δ^{13}C change obtained for core MD03-2698 is more reliable than that obtained for core CAR13-05.

From the modeling point of view, the 1° spatial resolution of the NorESM1-F model is not sufficient to correctly simulate a number of physical processes, like the coastal upwelling or deep overflows, with potential consequences for the simulated ocean circulation. Similarly, 1° ocean models cannot resolve the leaking Agulhas rings, which are crucial for the heat and salinity budget in the southeast Atlantic region. The Antarctic Circumpolar Current region is also prone to model bias (Beadling et al., 2020), and spurious open-ocean convection near the Weddell Sea (Heuzé, 2021) can lead to water mass biases in the Southern Ocean and beyond. In addition to these physical uncertainties, some uncertainties could also arise from the application to the glacial period of the BGC module with the same ecosystem parameterization as for the present, whereas there is evidence that some parameters, like the remineralization rate, should be temperature dependent (Brewer and Peltzer, 2017).

However, even though two of the three sites exhibiting model–data disagreement (red symbols) are located in the southeast Atlantic, no firm conclusion can be drawn regarding possible data or model biases due to the limited number of observations in the South Atlantic. When examining the geographical distribution of the three categories of sites, we find (i) model–data agreement (blue symbols) distributed over all latitudes, longitudes, and water depths; (ii) underestimated simulated changes (green symbols) in the North Atlantic, both along the western boundary current and the mid-Atlantic ridge and on the Iberian margin, at various water depths; and (iii) model–data disagreement (red symbols) below 3700 m in the North and South Atlantic, together with several blue sites and one green site. Therefore, the different categories of model–data agreement and/or disagreement do not correspond to any geographical pattern. This lack of geographical pattern points to the absence of obvious biases in the model results, at least in the North Atlantic.

To summarize, we obtain an overall good agreement between the change in δ^{13}C-BIO simulated by NorESM1-F and the observed change in *Cib.* δ^{13}C across the HS4-to-GI8 transition below 2000 m in the North Atlantic and equatorial West Atlantic (Fig. 1, Table 1).

4 Discussion

This overall good model–data agreement suggests that the model successfully reproduces the changes in ocean nutrients across a stadial–interstadial transition below 2000 m in the Atlantic Ocean. Moreover, it warrants the use of NorESM1-

F simulations to examine what caused the observed changes in *Cib.* δ^{13}C in that portion of the world ocean.

Prior to the stadial–interstadial transition, the simulated AMOC stream function is weak, with an upper overturning cell restrained to the upper 2000 m and a maximum overturning strength of about 10 Sv (Figs. 2a and S4). After the transition, the model results exhibit a strong overturning regime, with active deep-water formation in the northern North Atlantic and Nordic Seas leading to an upper overturning cell reaching down to $\sim$ 3000 m depth and a maximum overturning strength larger than 25 Sv (Figs. 2b and S4). This evolution of the simulated AMOC stream function is in agreement with the changes in overturning strength derived from the sedimentary Pa/Th records covering the HS4-to-GI8 transition (Henry et al., 2016; Waelbroeck et al., 2018). Moreover, even though the change in benthic δ^{18}O across the HS4-to-GI8 transition is very small and not significant for most sites, the simulated bottom-water-density decrease resulting from a slight bottom-water warming is in agreement with the observed benthic δ^{18}O decrease at the deep northeast Atlantic site U1308 (Sect. S4).

We use the simulated PO tracer defined as $PO = 172 \cdot PO_4 + O_2$ (Luo et al., 2018), similarly to the NO tracer first defined by Broecker (1974), to track the water mass origin. The PO tracer combines O_2 and PO_4 in such proportions that the increase in PO_4 by respiration is canceled, which makes this tracer nearly conservative. Given the difference in the preformed phosphate content of dense water produced in the northern and southern high latitudes of the Atlantic Ocean, SSWs and NSWs are characterized by high and low PO values, respectively. In our simulations of HS4 and GI8 ocean circulation, SSWs correspond to PO values above $\sim 0.55 \, \text{mol} \, O_2 \, \text{m}^{-3}$, and NSWs correspond to PO values below $\sim 0.45 \, \text{mol} \, O_2 \, \text{m}^{-3}$ (Fig. 2c and d).

Vertical sections of the PO tracer along the western basin before and after the HS4-to-GI8 transition show that NSWs were confined to the upper 2000 m before the transition, whereas active deep-water formation in the northern North Atlantic and Nordic Seas is clearly visible after the transition, with low PO values delimiting a North Atlantic Deep Water (NADW)-like water mass (Fig. 2c and d). This is further illustrated in horizontal PO maps at different water depths (Fig. 3), where the resumption of the southward-flowing deep western boundary current in the North Atlantic is reflected by low PO values down to 3500 m depth in the post-transition sections (Fig. 3e–h).

Importantly, as expected, changes in the spatial distribution of the PO tracer across the HS4-to-GI8 transition are remarkably similar to those of the preformed PO_4, both vertically (Fig. 2c–f) and horizontally (Figs. 3 and S5). This constitutes a validation of our use of PO_4^{pre} to assess the portion of the change in δ^{13}C-BIO from changes in ocean circulation and surface PP and further indicates that the changes in surface PP do not lead to a visible imprint on the interior ocean δ^{13}C-BIO distribution. The simulated PP

increase in some regions across the HS4-to-GI8 transition is indeed too weak to significantly draw down the PO_4^{pre} values and is not sufficient to prevent PO_4^{pre} from increasing in the same regions across the transition (Fig. S6). For simplicity, here, we thus simply interpret PO_4^{pre} in terms of changes in ocean circulation – that is, changes in water mass origin and geometry.

In addition, the NorESM1-F model computes the total oxygen utilization (TOU; Figs. 2g, h and 4), that is, the total oxygen consumed by organic matter remineralization, which translates into the amount of PO_4 locally produced by remineralization, PO_4^{rem} (Eq. 2). Increases in TOU or PO_4^{rem} thus correspond to decreases in δ^{13}C-BIO. Although the spatial distribution of the TOU before and after the HS4-to-GI8 transition is imprinted by the low TOU values of the NSW in the North Atlantic, it is markedly different from that of ocean circulation changes shown by PO_4^{pre} or the PO tracer in the South Atlantic (Figs. 2–4).

To summarize, PO_4^{pre} (or the PO tracer) on the one hand and PO_4^{rem} (or TOU) on the other hand give us access to the partitioning of the δ^{13}C-BIO change across the HS4-to-GI8 transition into the following two constituents: (i) the fraction change resulting from changes in water mass origin and geometry, and (ii) the complementary fraction caused by changes in remineralization (Eq. 3).

Based on the simulated PO_4^{pre} averaged over the previously defined HS4 and GI8 100-year intervals, we compute the portion of the GI8–HS4 δ^{13}C-BIO change due to ocean circulation changes, $(\Delta\delta^{13}\text{C-BIO})_{\text{circ}+\text{PP}}$, at the 18 selected sites. We find that the 11 sites located above 4200 m that exhibit significant GI8–HS4 δ^{13}C-BIO changes all show an increase in δ^{13}C-BIO across the transition. In these sites, $(\Delta\delta^{13}\text{C-BIO})_{\text{circ}+\text{PP}}$ forms 30 % to 90 % of the total GI8–HS4 δ^{13}C-BIO increase (Table 1). Furthermore, we find a loose, but significant ($R^2 = 0.64$), linear correlation, whereby the fraction change resulting from ocean circulation changes increases from ~ 40 % at 2000 m to ~ 80 % at 4000 m (Fig. S7). $(\Delta\delta^{13}\text{C-BIO})_{\text{rem}}$ thus forms 10 % to 70 % of the total GI8–HS4 δ^{13}C-BIO increase in these 11 sites (Table 1), with this fraction increasing with depth from ~ 20 % at 4000 m to ~ 60 % at 2000 m. The model results further show that the increase in δ^{13}C-BIO$_{\text{rem}}$ across the transition results from a decrease in remineralization explained by the stronger overturning circulation during GI8 than during HS4, which translates into shorter water mass residence times at these 11 sites, as shown by the decrease in ideal age at these sites across the transition (Fig. S8).

This increase in δ^{13}C-BIO$_{\text{circ}+\text{PP}}$ at the core sites located above 4200 m corresponds to an increase in the ratio of NSW versus SSW, as illustrated by the PO maps (Fig. 3). The largest changes occur in sites where SSW is replaced by NSW as a result of the resumption of deep-water formation in the northern high latitudes and the penetration of NADW-like NSW down to 3500 m in the northwest Atlantic and toward 30° S in the South Atlantic around 2500 m (Fig. 3).
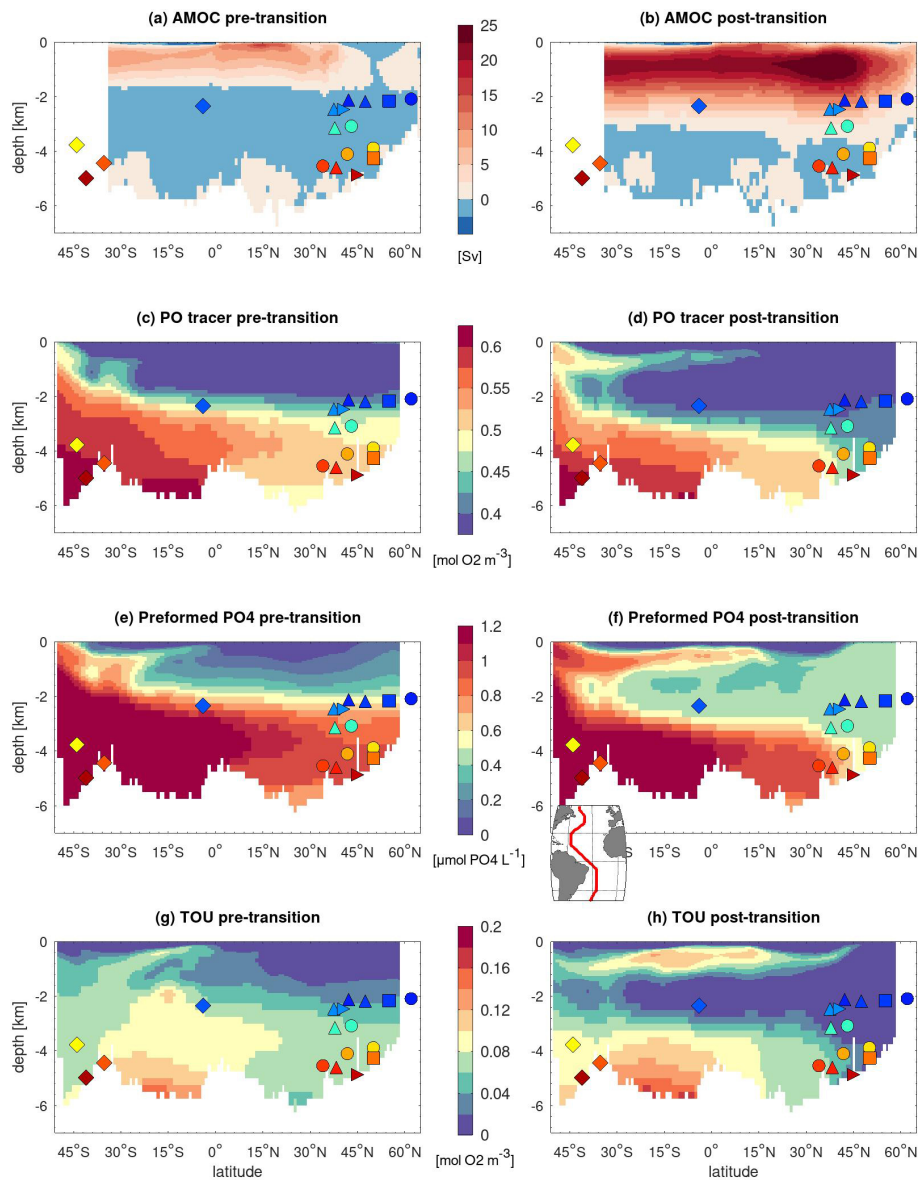
Figure 2. NorESM1-F simulated changes in Atlantic ocean circulation and nutrients across the HS4-to-GI8 transition. Pre- and post-transition values respectively correspond to 100-year averages over model years 5700–5800 of the simulation with freshwater forcing and model years 5950–6050 of the simulation in which the freshwater input has been halted. **(a, b)** Zonally integrated stream function. **(c–h)** Section plots along the western Atlantic section depicted in the inset. Colored symbols indicate the core sites as plotted in Fig. S1 and defined in Table 1.

Contrary to the δ^{13}C-BIO increase of up to 0.80‰ found in sites above 4200 m, δ^{13}C-BIO decreases by 0.02‰ to 0.12‰ across the HS4-to-GI8 transition in the six sites located below 4200 m (Fig. S9). At these deep sites, remineralization increases across the HS4-to-GI8 transition, leading to a 0.04‰ to 0.18‰ decrease in δ^{13}C-BIO$_{rem}$ (Eq. 3, Table 1). In contrast, the change in δ^{13}C-BIO$_{circ+PP}$ at these six deep sites is very small and barely significant (within -0.03‰ to $+0.02$‰), except in two southeast Atlantic sites, where it reaches $+0.06$‰ and $+0.08$‰but is counteracted

by larger decreases in the δ^{13}C-BIO$_{rem}$ component, reaching -0.18‰ and -0.14‰, respectively (Table 1). Such a decrease in δ^{13}C-BIO$_{rem}$ results from an increase in respired PO$_4$ and hence in organic matter export from the euphotic zone to the deep ocean during GI8 with respect to HS4. In particular, in our two subantarctic sites located below 4200 m, NorESM1-F simulates higher remineralization during interstadials than during stadials, which is consistent with an increased export production from the upper ocean to the deep Southern Ocean during interstadials, as demonstrated in
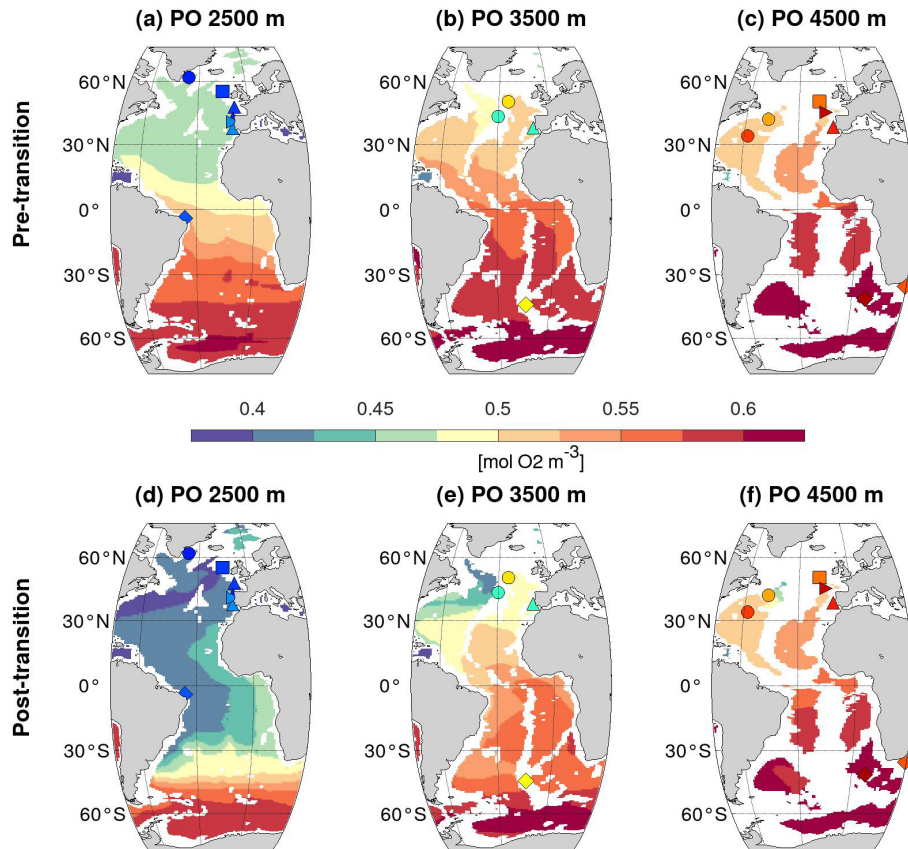
Figure 3. Same as Fig. 2 but for simulated PO tracer [mol O$_2$ m^{-3}] at 2500, 3500, and 4500 m depth in the Atlantic Ocean.

a number of studies (e.g., Gottschalk et al., 2016a; Martínez-García et al., 2014).

In addition to the above discussion of our model results at the selected 18 sites, the simulated maps of $\Delta\delta^{13}$C-BIO and of its partitioning into $(\Delta\delta^{13}$C-BIO$)_{\text{circ+PP}}$ and $(\Delta\delta^{13}$C-BIO$)_{\text{rem}}$ provide acceptable approximations of the change in *Cib.* δ^{13}C and of its partitioning into a circulation and surface PP term on one hand and a remineralization term on the other hand anywhere below 2000 m in the Atlantic Ocean (Fig. S10).

It is tempting to compare our results with a recent study of the LGM-to-HS1 transition by Gu et al. (2021), who concluded that the δ^{13}C-DIC decrease observed at mid-depth is mainly explained by increased remineralization due to AMOC slowdown, while the water mass mixture change plays only a minor role. However, Gu et al. (2021) used a transient simulation of the last deglaciation to examine the causes of the mid-depth Atlantic δ^{13}C-DIC decrease observed across the transition from the LGM into the HS1 stadial, whereas we use a hosing experiment under constant radiative forcing to examine the transition from the HS4 stadial to the GI8 interstadial, away from the last deglaciation and its large changes in radiative forcing. The results of the two studies can thus hardly be compared. Despite these different

settings, both studies show that the remineralization changes due to ventilation changes are the main factor contributing to the observed Atlantic δ^{13}C-DIC change at about 2000 m water depth. But this agreement does not hold at greater depths, where our results suggest that water mass mixture change is the main factor of the Atlantic δ^{13}C-DIC change between $\sim$ 2500 and 4000 m.

5 Conclusions

We show that the observed *Cib.* δ^{13}C changes across the HS4-to-GI8 stadial–interstadial transition can be successfully approximated by the computed change in dissolved inorganic carbon δ^{13}C, $\Delta\delta^{13}$C-BIO, assuming no change in air–sea exchanges and using the nutrient fields simulated by the NorESM1-F model across a stadial–interstadial transition.

The model results can then be used to gain insight into the causes of the observed *Cib.* δ^{13}C change across the HS4-to-GI8 transition and to assess the fraction of the change resulting from changes in water mass origin and geometry on the one hand and that associated with changes in organic matter remineralization in the interior ocean on the other hand. Above $\sim$ 4200 m, a large fraction of the computed δ^{13}C-BIO
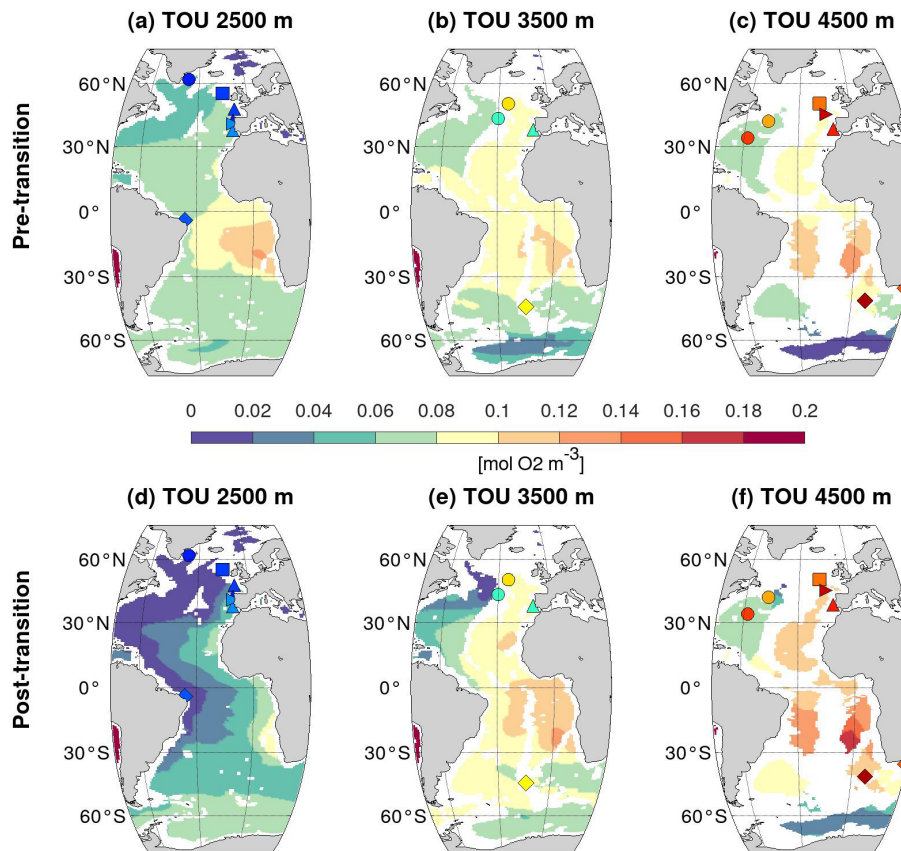
Figure 4. Same as Fig. 3 but for simulated total oxygen utilization (mol O_2 m^{-3}) at 2500, 3500, and 4500 m depth in the Atlantic Ocean.

increase results from the replacement of SSW by NSW subsequent to the resumption of deep-water formation in the northern high latitudes after the freshwater input is halted. This fraction exhibits a loose linear relationship with depth, increasing from $\sim 40\%$ at 2000 m to $\sim 80\%$ at 4000 m. Conversely, the δ^{13}C-BIO increase resulting from the decrease in remineralization across the HS4-to-GI8 transition in response to the faster flow rates during GI8 than during HS4 represents $\sim 60\%$ of the δ^{13}C-BIO increase at 2000 m but only $\sim 20\%$ of the δ^{13}C-BIO increase at 4000 m.

Below ~ 4200 m, the model shows little change in δ^{13}C-BIO resulting from changes in water mass origin and geometry but an increase in remineralization across the HS4-to-GI8 transition. The simulated lower remineralization during stadials than during interstadials is particularly pronounced in our deep subantarctic sites, which is in agreement with the decrease in the biological export production during stadials found in the Southern Ocean in previous studies.

Author contributions. CW, JT, CG, and KN designed the research. CG performed the model run. JT contributed expert knowledge on the biogeochemical model component. JT and CW made the figures. NVR contributed expert advice to an earlier version of this paper. ST, FE, SL, and SN provided sedimentology expertise and access to cores MD13-3438 and MD03-2698. FD supervised and quality-controlled all the ACCLIMATE isotopic data. LR performed the planktonic foraminifera census counts on core MD13-3438. EM performed the grain size analysis on core CAR2013-PQP-CAR05. CW, JT, and CG wrote the paper, with contributions from all the co-authors.

References

Beadling, R. L., Russell, J., Stouffer, R., Mazloff, M., Talley, L., Goodman, P., Sallée, J.-B., Hewitt, H., Hyder, P., and Pandde, A.: Representation of Southern Ocean properties across coupled model intercomparison project generations: CMIP3 to CMIP6, J. Climate, 33, 6555–6581, 2020.

Bernardello, R., Marinov, I., Palter, J. B., Sarmiento, J. L., Galbraith, E. D., and Slater, R. D.: Response of the ocean natural carbon storage to projected twenty-first-century climate change, J. Climate, 27, 2033–2053, 2014.

Brewer, P. G. and Peltzer, E. T.: Depth perception: the need to report ocean biogeochemical rates as functions of temperature, not depth, Philos. T. Roy. Soc. A, 375, 20160319, https://doi.org/10.1098/rsta.2016.0319, 2017.

Broecker, W. S.: 'NO', a conservative water mass tracer, Earth Planet Sc. Lett., 23, 100–107, 1974.

Broecker, W. S. and Maier-Reimer, E.: The influence of air and sea exchange on the carbon isotope distribution in the sea, Global Biogeochem. Cy., 6, 315–320, 1992.

Crocker, A. J., Chalk, T. B., Bailey, I., Spencer, M. R., Gutjahr, M., Foster, G. L., and Wilson, P. A.: Geochemical response of the mid-depth Northeast Atlantic Ocean to freshwater input during Heinrich events 1 to 4, Quaternary Sci. Rev., 151, 236–254, 2016.

Duplessy, J.-C., Shackleton, N. J., Matthews, R. K., Prell, W., Ruddiman, W. F., Caralp, M., and Hendy, C. H.: ^{13}C record of benthic foraminifera in the last interglacial ocean: implications for the carbon cycle and the global deep water circulation, Quatern. Res., 21, 225–243, 1984.

Duplessy, J.-C., Shackleton, N. J., Fairbanks, R. G., Labeyrie, L., Oppo, D., and Kallel, N.: Deepwater source variations during the last climatic cycle and their impact on the global deepwater circulation, Paleoceanography, 3, 343–360, 1988.

Duteil, O., Koeve, W., Oschlies, A., Aumont, O., Bianchi, D., Bopp, L., Galbraith, E., Matear, R., Moore, J. K., Sarmiento, J. L., and Segschneider, J.: Preformed and regenerated phosphate in ocean general circulation models: can right total concentrations be wrong?, Biogeosciences, 9, 1797–1807, https://doi.org/10.5194/bg-9-1797-2012, 2012.

Eide, M., Olsen, A., Ninnemann, U. S., and Johannessen, T.: A global ocean climatology of preindustrial and modern ocean δ^{13}C, Global Biogeochem. Cy., 31, 515–534, 2017.

Elliot, M., Labeyrie, L., and Duplessy, J. C.: Changes in North-Atlantic deep-water formation associated with the Dansgaard-Oeschger temperature oscillations (60–10 ka), Quaternary Sci. Rev., 21, 1153–1165, 2002.

Galaasen, E. V., Ninnemann, U. S., Kessler, A., Irvalı, N., Rosenthal, Y., Tjiputra, J., Bouttes, N., Roche, D. M., Kleiven, H. F., and Hodell, D. A.: Interglacial instability of North Atlantic deep water ventilation, Science, 367, 1485–1489, 2020.

Garcia, H., Locarnini, R., Boyer, T., Antonov, J., Zweng, M., Baranova, O., and Johnson, D.: Dissolved oxygen, apparent oxygen utilization, and oxygen saturation, in: World Ocean Atlas 2009, edited by: Levitus, S., NOAA Atlas NESDIS 70, US Government Printing Office, Washington, DC, USA, 344 pp., https://www.ncei.noaa.gov/sites/default/files/2020-04/woa09_vol3_text.pdf (last access: 2 May 2023), 2010a.

Garcia, H., Locarnini, R., Boyer, T., Antonov, J., Zweng, M., Baranova, O., and Johnson, D.: Nutrients (phosphate, nitrate, silicate), in: World Ocean Atlas 2009, edited by: Levitus, S., NOAA Atlas NESDIS 71, US Government Printing Office, Washington, DC, USA, 398 pp., https://www.ncei.noaa.gov/sites/default/files/2020-04/woa09_vol4_text.pdf (last access: 2 May 2023), 2010b.

Gebbie, G., Peterson, C. D., Lisiecki, L. E., and Spero, H. J.: Global-mean marine δ^{13}C and its uncertainty in a glacial state estimate, Quaternary Sci. Rev., 125, 144–159, 2015.

Gottschalk, J., Skinner, L. C., Misra, S., Waelbroeck, C., Menviel, L., and Timmermann, A.: Abrupt changes in the southern extent of North Atlantic Deep Water during Dansgaard–Oeschger events, Nat. Geosci., 8, 950–954, https://doi.org/10.1038/ngeo2558, 2015.

Gottschalk, J., Skinner, L. C., Lippold, J., Vogel, H., Frank, N., Jaccard, S. L., and Waelbroeck, C.: Biological and physical controls in the Southern Ocean on past millennial-scale atmospheric CO_2 changes, Nat. Commun., 7, 11539, https://doi.org/10.1038/ncomms11539, 2016a.

Gottschalk, J., Vázquez Riveiros, N., Waelbroeck, C., Skinner, L. C., Michel, E., Duplessy, J. C., Hodell, D., and Mackensen, A.: Carbon isotope offsets between benthic foraminifer species of the genus Cibicides (Cibicidoides) in the glacial sub-Antarctic Atlantic, Paleoceanography, 31, 1583–1602, 2016b.

Gu, S., Liu, Z., Oppo, D. W., Lynch-Stieglitz, J., Jahn, A., Zhang, J., Lindsay, K., and Wu, L.: Remineralization dominating the δ^{13}C decrease in the mid-depth Atlantic during the last deglaciation, Earth Planet. Sc. Lett., 571, 117106, https://doi.org/10.1016/j.epsl.2021.117106, 2021.

Guo, C.: Arctic circulation changes at the transition from a Heinrich stadial to a Greenland interstadial, in preparation, 2023.

Guo, C., Bentsen, M., Bethke, I., Ilicak, M., Tjiputra, J., Toniazzo, T., Schwinger, J., and Otterå, O. H.: Description and evaluation of NorESM1-F: a fast version of the Norwegian Earth System Model (NorESM), Geosci. Model Dev., 12, 343–362, https://doi.org/10.5194/gmd-12-343-2019, 2019a.

Guo, C., Nisancioglu, K. H., Bentsen, M., Bethke, I., and Zhang, Z.: Equilibrium simulations of Marine Isotope Stage 3 climate, Clim. Past, 15, 1133–1151, https://doi.org/10.5194/cp-15-1133-2019, 2019b.

Henry, L., McManus, J. F., Curry, W. B., Roberts, N. L., Piotrowski, A. M., and Keigwin, L. D.: North Atlantic ocean circulation and abrupt climate change during the last glaciation, Science, 353, 470–474, https://doi.org/10.1126/science.aaf5529, 2016.

Heuzé, C.: Antarctic Bottom Water and North Atlantic Deep Water in CMIP6 models, Ocean Sci., 17, 59–90, https://doi.org/10.5194/os-17-59-2021, 2021.

Hoogakker, B., McCave, I., and Vautravers, M.: Antarctic link to deep flow speed variation during Marine Isotope Stage 3 in the western North Atlantic, Earth Planet. Sc. Lett., 257, 463–473, 2007.

Jansen, E., Christensen, J. H., Dokken, T., Nisancioglu, K. H., Vinther, B. M., Capron, E., Guo, C., Jensen, M. F., Langen, P. L., and Pedersen, R. A.: Past perspectives on the present era of abrupt Arctic climate change, Nat. Clim. Change, 10, 714–721, 2020.

Kessler, A., Galaasen, E. V., Ninnemann, U. S., and Tjiputra, J.: Ocean carbon inventory under warmer climate conditions – the case of the Last Interglacial, Clim. Past, 14, 1961–1976, https://doi.org/10.5194/cp-14-1961-2018, 2018.

Key, R. M., Kozyr, A., Sabine, C. L., Lee, K., Wanninkhof, R., Bullister, J. L., Feely, R. A., Millero, F. J., Mordy, C., and Peng, T. H.: A global ocean carbon climatology: Results from Global Data Analysis Project (GLODAP), Global Biogeochem. Cy., 18, 1–23, 2004.

Lacerra, M., Lund, D., Yu, J., and Schmittner, A.: Carbon storage in the mid-depth Atlantic during millennial-scale climate events, Paleoceanography, 32, 780–795, 2017.

Lougheed, B. C., Waelbroeck, C., Smialkowski, N., Vazquez Riveiros, N., and Obrochta, S. P.: A Simplified Palaeoceanography Archiving System (PARIS) and GUI for Storage and Visualisation of Marine Sediment Core Proxy Data vs Age and Depth, Open Quatern., 8, 1–11, https://doi.org/10.5334/oq.101, 2022.

Lund, D., Tessin, A., Hoffman, J., and Schmittner, A.: Southwest Atlantic water mass evolution during the last deglaciation, Paleoceanography, 30, 477–494, 2015.

Luo, Y., Tjiputra, J., Guo, C., Zhang, Z., and Lippold, J.: Atlantic deep water circulation during the last interglacial, Sci. Rep., 8, 1–8, 2018.

Lynch-Stieglitz, J. and Marchitto, T. M.: Tracers of past ocean circulation, in: The Oceans and Marine Geochemistry, edited by: Mottl, M. and Elderfield, H., Elsevier, Amsterdam, 433–451, https://doi.org/10.1016/B978-0-08-095975-7.00616-1, 2014.

Lynch-Stieglitz, J., Stocker, T., Broecker, W. S., and Fairbanks, R. G.: The influence of air-sea exchange on the isotopic composition of oceanic carbon: Observations and modeling, Global Biogeochem. Cy., 9, 653–665, 1995.

Mackensen, A., Hubberten, H. W., Bickert, T., Fischer, G., and Fütterer, D.: The δ^{13}C in benthic foraminiferal tests of Fontbotia wuellerstorfi (Schwager) relative to the δ^{13}C of dissolved inorganic carbon in southern ocean deep water: implications for glacial ocean circulation models, Paleoceanography, 8, 587–610, 1993.

Martínez-García, A., Sigman, D. M., Ren, H., Anderson, R. F., Straub, M., Hodell, D. A., Jaccard, S. L., Eglinton, T. I., and Haug, G. H.: Iron fertilization of the Subantarctic Ocean during the last ice age, Science, 343, 1347–1350, 2014.

Menviel, L., Mouchet, A., Meissner, K. J., Joos, F., and England, M. H.: Impact of oceanic circulation changes on atmospheric $\delta^{13}CO_2$, Global Biogeochem. Cy., 29, 1944–1961, 2015.

Menviel, L., Yu, J., Joos, F., Mouchet, A., Meissner, K., and England, M. H.: Poorly ventilated deep ocean at the Last Glacial Maximum inferred from carbon isotopes: A data-model comparison study, Paleoceanography, 32, 2–17, 2017.

Menviel, L., Spence, P., Skinner, L., Tachikawa, K., Friedrich, T., Missiaen, L., and Yu, J.: Enhanced Mid-depth Southward Transport in the Northeast Atlantic at the Last Glacial Maximum Despite a Weaker AMOC, Paleoceanogr. Paleoclim., 35, e2019PA003793, https://doi.org/10.1029/2019PA003793, 2020.

Missiaen, L., Bouttes, N., Roche, D. M., Dutay, J.-C., Quiquet, A., Waelbroeck, C., Pichat, S., and Peterschmitt, J.-Y.: Carbon isotopes and Pa/Th response to forced circulation changes: a model perspective, Clim. Past, 16, 867–883, https://doi.org/10.5194/cp-16-867-2020, 2020.

Morée, A. L., Schwinger, J., Ninnemann, U. S., Jeltsch-Thömmes, A., Bethke, I., and Heinze, C.: Evaluating the biological pump efficiency of the Last Glacial Maximum ocean using δ^{13}C, Clim. Past, 17, 753–774, https://doi.org/10.5194/cp-17-753-2021, 2021.

Muglia, J. and Schmittner, A.: Carbon isotope constraints on glacial Atlantic meridional overturning: strength vs depth, Quaternary Sci. Rev., 257, 106844, https://doi.org/10.1016/j.quascirev.2021.106844, 2021.

Muglia, J., Skinner, L. C., and Schmittner, A.: Weak overturning circulation and high Southern Ocean nutrient utilization maximized glacial ocean carbon, Earth Planet. Sc. Lett., 496, 47–56, 2018.

Oppo, D. W., Curry, W. B., and McManus, J. F.: What do benthic δ^{13}C and δ^{18}O data tell us about Atlantic circulation during Heinrich Stadial 1?, Paleoceanography, 30, 353–368, 2015.

Peck, V. L., Hall, I. R., Zahn, R., Elderfield, H., Grousset, F., Hemming, S. R., and Scourse, J. D.: High resolution evidence for linkages between NW European ice sheet instability and Atlantic Meridional Overturning Circulation, Earth Planet. Sc. Lett., 243, 476–488, 2006.

Peck, V. L., Hall, I. R., Zahn, R., and Scourse, J. D.: Progressive reduction in NE Atlantic intermediate water ventilation prior to Heinrich events: Response to NW European ice sheet instabilities?, Geochem. Geophy. Geosy., 8, Q01N10, https://doi.org/10.1029/2006GC001321, 2007.

Rasmussen, S. O., Bigler, M., Blockley, S. P., Blunier, T., Buchardt, S. L., Clausen, H. B., Cvijanovic, I., Dahl-Jensen, D., Johnsen, S. J., and Fischer, H.: A stratigraphic framework for abrupt climatic changes during the Last Glacial period based on three synchronized Greenland ice-core records: refining and extending the IN-

TIMATE event stratigraphy, Quaternary Sci. Rev., 106, 14–28, 2014.

Schmittner, A. and Lund, D. C.: Early deglacial Atlantic overturning decline and its role in atmospheric CO_2 rise inferred from carbon isotopes (δ^{13}C), Clim. Past, 11, 135–152, https://doi.org/10.5194/cp-11-135-2015, 2015.

Schmittner, A., Gruber, N., Mix, A. C., Key, R. M., Tagliabue, A., and Westberry, T. K.: Biology and air–sea gas exchange controls on the distribution of carbon isotope ratios (δ^{13}C) in the ocean, Biogeosciences, 10, 5793–5816, https://doi.org/10.5194/bg-10-5793-2013, 2013.

Schmittner, A., Bostock, H. C., Cartapanis, O., Curry, W. B., Filipsson, H. L., Galbraith, E. D., Gottschalk, J., Herguera, J. C., Hoogakker, B., Jaccard, S. L., Lisiecki, L. E., Lund, D. C., Martínez-Méndez, G., Lynch-Stieglitz, J., Mackensen, A., Michel, E., Mix, A. C., Oppo, D. W., Peterson, C. D., Repschläger, J., Sikes, E. L., Spero, H. J., and Waelbroeck, C.: Calibration of the carbon isotope composition (δ^{13}C) of benthic foraminifera, Paleoceanography, 32, 512–530, https://doi.org/10.1002/2016PA003072, 2017.

Skinner, L. and Shackleton, N.: Deconstructing Terminations I and II: revisiting the glacioeustatic paradigm based on deepwater temperature estimates, Quaternary Sci. Rev., 25, 3312–3321, 2006.

Takahashi, T., Broecker, W. S., and Langer, S.: Redfield ratio based on chemical data from isopycnal surfaces, J. Geophys. Res.-Oceans, 90, 6907–6924, https://doi.org/10.1029/JC090iC04p06907, 1985.

Tjiputra, J. F., Schwinger, J., Bentsen, M., Morée, A. L., Gao, S., Bethke, I., Heinze, C., Goris, N., Gupta, A., He, Y.-C., Olivié, D., Seland, Ø., and Schulz, M.: Ocean biogeochemistry in the Norwegian Earth System Model version 2 (NorESM2), Geosci. Model Dev., 13, 2393–2431, https://doi.org/10.5194/gmd-13-2393-2020, 2020.

Toucanne, S., Soulet, G., Vázquez Riveiros, N., Boswell, S. M., Dennielou, B., Waelbroeck, C., Bayon, G., Mojtahid, M., Bosq, M., and Sabine, M.: The North Atlantic Glacial Eastern Boundary Current as a Key Driver for Ice-Sheet – AMOC Interactions and Climate Instability, Paleoceanogr. Paleoclimatol., 36, e2020PA004068, https://doi.org/10.1029/2020PA004068, 2021.

Vidal, L., Labeyrie, L., Cortijo, E., Arnold, M., Duplessy, J. C., Michel, E., Becqué, S., and van Weering, T. C. E.: Evidence for changes in the North Atlantic Deep Water linked to meltwater surges during the Heinrich events, Earth Planet. Sc. Lett., 146, 13–26, 1997.

Voigt, I., Cruz, A., Mulitza, S., Chiessi, C., Mackensen, A., Lippold, J., Antz, B., Zabel, M., Zhang, Y., and Barbosa, C.: Variability in mid-depth ventilation of the western Atlantic Ocean during the last deglaciation, Paleoceanography, 32, 948–965, 2017.

Waelbroeck, C., Skinner, L. C., Labeyrie, L., Duplessy, J.-C., Michel, E., Vazquez Riveiros, N., Gherardi, J.-M., and Dewilde, F.: The timing of deglacial circulation changes in the Atlantic, Paleoceanography, 26, PA3213, https://doi.org/10.1029/2010PA002007, 2011.

Waelbroeck, C., Pichat, S., Böhm, E., Lougheed, B. C., Faranda, D., Vrac, M., Missiaen, L., Vazquez Riveiros, N., Burckel, P., Lippold, J., Arz, H. W., Dokken, T., Thil, F., and Dapoigny, A.: Relative timing of precipitation and ocean circulation changes in the western equatorial Atlantic over the last 45 ky, Clim. Past, 14, 1315–1330, https://doi.org/10.5194/cp-14-1315-2018, 2018.

Waelbroeck, C., Lougheed, B. C., Vazquez Riveiros, N., Missiaen, L., Pedro, J., Dokken, T., Hajdas, I., Wacker, L., Abbott, P., Dumoulin, J.-P., Thil, F., Eynaud, F., Rossignol, L., Fersi, W., Albuquerque, A. L., Arz, H., Austin, W. E. N., Came, R., Carlson, A. E., Collins, J. A., Dennielou, B., Desprat, S., Dickson, A., Elliot, M., Farmer, C., Giraudeau, J., Gottschalk, J., Henderiks, J., Hughen, K., Jung, S., Knutz, P., Lebreiro, S., Lund, D. C., Lynch-Stieglitz, J., Malaizé, B., Marchitto, T., Martínez-Méndez, G., Mollenhauer, G., Naughton, F., Nave, S., Nürnberg, D., Oppo, D., Peck, V., Peeters, F. J. C., Penaud, A., Portilho-Ramos, R. d. C., Repschläger, J., Roberts, J., Rühlemann, C., Salgueiro, E., Sanchez Goni, M. F., Schönfeld, J., Scussolini, P., Skinner, L. C., Skonieczny, C., Thornalley, D., Toucanne, S., Rooij, D. V., Vidal, L., Voelker, A. H. L., Wary, M., Weldeab, S., and Ziegler, M.: Consistently dated Atlantic sediment cores over the last 40 thousand years, Scient. Data, 6, 165, https://doi.org/10.1038/s41597-019-0173-8, 2019.

Waelbroeck, C., Tjiputra, J., Guo, C., Nisancioglu, K. H., Jansen, E., Vazquez Riveiros, N., Toucanne, S., Eynaud, F., Rossignol, L., Dewilde, F., Marches, E., Lebreiro, S., and Nave, S.: Atlantic circulation changes across a stadial-interstadial transition, SEANOE [data set], https://doi.org/10.17882/91130, 2022.

Willamowski, C. and Zahn, R.: Upper ocean circulation in the glacial North Atlantic from benthic foraminiferal isotopie and trace element fingerprinting, Paleoceanography, 15, 515–527, 2000.

Wolff, E. W., Chappellaz, J., Blunier, T., Rasmussen, S. O., and Svensson, A.: Millennial-scale variability during the last glacial: The ice core record, Quaternary Sci. Rev., 29, 2828–2838, 2010.

Zahn, R., Winn, K., and Sarnthein, M.: Benthic foraminiferal δ^{13}C and accumulation rates of organic carbon: Uvigerina peregrina group and Cibicidoides wuellerstorfi, Paleoceanography, 1, 27–42, 1986.